

Simulation of deuterium pellet ablation and deposition in the EAST tokamak with HPI2 code

Da-Zheng Li(李大正), Jie Zhang(张洁), Ji-Lei Hou(侯吉磊), Mao Li(李懋), and Ji-Zhong Sun(孙继忠)

Citation: Chin. Phys. B, 2024, 33 (**4**): 045204. DOI: 10.1088/1674-1056/ad1e68
Journal homepage: http://cpb.iphy.ac.cn; http://iopscience.iop.org/cpb

What follows is a list of articles you may be interested in

Numerical study of alpha particle loss with toroidal field ripple based on CFETR steady-state scenario

Niuqi Li(李钮琦), Yingfeng Xu(徐颖峰), Fangchuan Zhong(钟方川), and Debing Zhang(张德兵)
Chin. Phys. B, 2024, 33 (**1**): 015202. DOI: 10.1088/1674-1056/ad03de

Stability impacts from the current and pressure profile modifications within finite sized island

Yuxiang Sun(孙宇翔) and Di Hu(胡地)
Chin. Phys. B, 2023, 32 (**7**): 075212. DOI: 10.1088/1674-1056/acd369

Drift surface solver for runaway electron current dominant equilibria during the current quench

Lu Yuan(袁露) and Di Hu(胡地)
Chin. Phys. B, 2023, 32 (**7**): 075208. DOI: 10.1088/1674-1056/acc1d7

Parametric decay instabilities of lower hybrid waves on CFETR

Taotao Zhou(周涛涛), Nong Xiang(项农), Chunyun Gan(甘春芸), Guozhang Jia(贾国章), and Jiale Chen(陈佳乐)
Chin. Phys. B, 2022, 31 (**9**): 095201. DOI: 10.1088/1674-1056/ac67c2

Numerical simulation of fueling pellet ablation and transport in the EAST H-mode discharge

Wan-Ting Chen(陈婉婷), Ji-Zhong Sun(孙继忠), Fang Gao(高放), Lei Peng(彭磊), and De-Zhen Wang(王德真)
Chin. Phys. B, 2022, 31 (**7**): 075204. DOI: 10.1088/1674-1056/ac5c35

Simulation of deuterium pellet ablation and deposition in the EAST tokamak with HPI2 code

Da-Zheng Li(李大正)[1], Jie Zhang(张洁)[2,†], Ji-Lei Hou(侯吉磊)[3], Mao Li(李懋)[1], and Ji-Zhong Sun(孙继忠)[1,‡]

[1] *Key Laboratory of Materials Modification by Laser, Ion, and Electron Beams (Ministry of Education), School of Physics, Dalian University of Technology, Dalian* 116024, *China*

[2] *Department of Plasma Physics and Fusion Engineering, University of Science and Technology of China, Hefei* 230026, *China*

[3] *Institute of Plasma Physics, Chinese Academy of Sciences, Hefei* 230031, *China*

(Received 9 November 2023; revised manuscript received 27 December 2023; accepted manuscript online 15 January 2024)

Pellet injection is a primary method for fueling the plasma in magnetic confinement devices. For that goal the knowledges of pellet ablation and deposition profiles are critical. In the present study, the pellet fueling code HPI2 was used to predict the ablation and deposition profiles of deuterium pellets injected into a typical H-mode discharge on the EAST tokamak. Pellet ablation and deposition profiles were evaluated for various pellet injection locations, with the aim at optimizing the pellet injection to obtain a deep fueling depth. In this study, we investigate the effect of the injection angle on the deposition depth of the pellet at different velocities and sizes. The ablation and deposition of the injected pellet are mainly studied at each injection position for three different injection angles: 0°, 45°, and 60°. The pellet injection on the high field side (HFS) can achieve a more ideal deposition depth than on the low field side (LFS). Among these angles, horizontal injection on the middle plane is relatively better on either the HFS or the LFS. When the injection location is 0.468 m below the middle plane on the HFS or 0.40 m above the middle plane of the LFS, it can achieve a similar deposition depth to the one of its corresponding side. When the pre-cooling effect is taken into account, the deposition depth is predicted to increase only slightly when the pellet is launched from the HFS. The findings of this study will serve as a reference for the update of pellet injection systems for the EAST tokamak.

Keywords: pellet injection, pellet ablation, HPI2, pellet deposition

PACS: 52.55.Fa, 52.65.–y **DOI:** 10.1088/1674-1056/ad1e68

1. Introduction

Nuclear fusion energy is a highly efficient and eco-friendly source of renewable energy. Among all nuclides for fusion, deuterium and tritium have the largest fusion reaction cross-section at a relatively low energy. Therefore, most efforts are put into achieving D–T fusion reaction. The fusion reactors to be built in the near future also relies mainly on deuterium and tritium fusion reaction. In a burning plasma, The fuel of D and T needs to be supplied to replenish the fuel not only due to nuclear fusion reaction consumption but also due to particle loss induced by various processes, such as the pumping out effect induced by the edge localized modes (ELMs), and pumping for ash and impurity removal.[1]

There are several fueling methods, such as supersonic molecular beam injection (SMBI),[2] gas puffing (GP),[3] and pellet injection (PI).[4] As a key tool for providing a deep fueling, PI technology has been widely recognized to be more suitable for future fusion devices.[5–8] It is commonly used in current magnetic confinement fusion devices, such as DIII-D,[9] JT-60U,[10] HL-2A,[11] Tore Supra,[12] Alcator C-mod,[13] and EAST.[14,15] In 2012, a pellet fueling system with a frequency of 10 Hz was successfully developed for the EAST tokamak. This system produces cylindrical pellets of around 2.0 mm in both length and diameter.[16] A typical pellet contains around 3.8×10^{20} particles. In addition, the pellet injection system on EAST are capable of injecting the pellet both from the high field side (HFS) and the low field side (LFS) at a velocity of 100–300 m·s^{-1} with a maximum injection frequency of 10 Hz.[17] PI is also the preferred injection method for the future fusion reactors such as ITER. This method requires a highly integrated pellet injection system that applies vacuum, low-temperature, and high-pressure technologies. Currently, the fueling efficiency of PI ranges typically from 30% to 90% for present devices. However, in future devices the fueling efficiency is expected to be low due to shallow pellet penetration in the very high temperature edge plasma and the resulting shallow particle deposition. This poses a main challenge to the design of future fusion devices. Therefore, research on pellet source modeling and optimization of pellet injection parameters to achieve deep fueling depth is of significant importance.

Pellet source modeling includes two main processes: pellet ablation and homogenization. Parks developed the neutral gas shielding (NGS) model for pellet ablation,[18] which relates the pellet ablation rate with the background electron temperature and density, pellet injection speed and pellet size. The NGS model considers the formation of a neutral cloud around the pellet surface when the pellet enters the high tem-

†Corresponding author. E-mail: jiez111@ustc.edu.cn

‡Corresponding author. E-mail: jsun@dlut.edu.cn

© 2024 Chinese Physical Society and IOP Publishing Ltd

perature plasma. The neutral cloud acts as a protective shield against the heat flux from the background plasma, thereby enhancing the pellet penetration depth. Results obtained with the NGS model has been validated by comparing with the experimental data, such as those from the International Pellet Ablation Data Base (IPADBASE).[19] At present, numerical simulations have already been conducted to study the pellet penetration and particle deposition depth in EAST discharges with numerical codes, for example, dynamic neutral gas shielding model coupled with SOLPS-ITER[20,21] and the PAM[22,23] code. The latter implements an areal deposition model and a 2D Gaussian deposition model, which resolves well the tangential singularity problem, encountered when the pellet trajectory aligns with a magnetic flux surface. However, these two codes adopt scaling laws for reducing the computational costs, and correspondingly, the codes do not run in a self-consistent way with the pellet ablation and deposition, and neglects many sophisticated physical processes.[23,24] In this work, the HPI2 code is utilized to simulate the pellet ablation and deposition based on first principles. The pellet ablation simulation in HPI2 is based on the neutral gas and plasma shielding (NGPS) model,[19,25,26] which is further developed on the basis of the NGS model. In addition to the neutral cloud shielding, the NGPS model considers the extra shielding from the cold plasma cloud formed of ablated particles, which expands along the magnetic field. The cold plasma cloud is also called "plasmoid", which will detach from the pellet and drift along the major radius of the tokamak.[26] Especially, with consideration of the ∇B-induced drift, simulation of pellet ablation becomes more self-consistent, since the plasmoid length is limited to be finite by the drift. Therefore, we applied the HPI2 code to the EAST device to study its pellet injection.

The remaining part of the present paper is organized as follows: Section 2 introduces the background plasma information of a typical H-mode discharge on the EAST tokamak and the simulation setup. Section 3 presents the simulation results of pellet ablation and deposition with various pellet injection parameters, and provides an in-depth analysis and discussion. Section 4 summarizes our findings.

2. Simulation details

2.1. HPI2 code

The HPI2 pellet code offers the flexibility to run within a transport code such as CRONOS, JINTRAC, or ETS, enabling the calculation of source profiles associated with pellet injection events, or it can operate independently in standalone mode.[27,28] The hydrogen isotopes pellet injection code HPI2 is based on a two-cell four-fluid Lagrangian model for plasmoid evolution.[29] The two cells refer to the background plasma and the plasmoid, while the four fluids refer to electrons and ions in two cells, respectively.[27,28,30–32] As soon as the plasmoid particles are ionized, they experience the Lorentz force that stops both their radial expansion and motion across the plasma. The motional electric field (induced by $v_\mathrm{p} \times B$, where v_p is pellet velocity and ablated particles have a velocity component equal to v_p) in the pellet reference frame tends to cancel the component that stops the motion through the plasma, but, simultaneously, the ∇B-induced drift provokes the drift of the plasmoid down the magnetic field gradient. It results that the plasmoid drifts down ∇B starting from an initial velocity equal to the pellet velocity (for incomplete ionization, the drift velocity is taken to be the weighted average between the ionized population which experiences the drift and the neutrals that tend to follow the pellet). A plasmoid is ejected as soon as the distance covered by this effective drift becomes equal to the cloud radius. Once a plasmoid has detached from the ablation cloud, a diffusive approximation is used for calculating the energy transfer from the background plasma. Both parallel and perpendicular fluxes are taken into account, including the increase of the corresponding plasmoid surfaces due to cross-field diffusion and magnetic shear. The evolution of the plasmoid parameters (dimensions, density and ion and electron temperatures) are calculated through 0D equations described in Refs. [32,33]. The finite size of the magnetic flux shell in which the plasmoid homogenizes is taken into account (i.e., the background plasma is compressed due to the plasmoid expansion and its temperature decreases due to the energy transfer to the plasmoid). In terms of the ∇B-induced drift, various drift damping mechanisms have been taken into account, such as Alfvén wave propagation and the effects of parallel resistive currents both outside (known as the Pégourié effects) and within the plasmoid (known as the Rozhansky effects).[34–36] From the 0D-modelling, it follows that the drift displacement is a value averaged over the whole plasmoid. At each time step, the corresponding displacement is applied at every point of the plasmoid, depending on its poloidal position. Details about the HPI2 code can be found in Ref. [33].

The HPI2 code is a powerful tool that enables accurate trajectory calculations for pellet injection in 2D magnetic flux coordinates. It takes into account various complex physical processes such as pre-cooling effect, pellet rocket acceleration effect, and the impact of fast ions or electrons on pellet ablation.[33] Based on the NGPS model, this code provides a detailed analysis of the homogenization process, tracking the time evolution of the plasmoid and calculating its drift displacement. Moreover, the code is very adaptable and can examine different pellet injection scenarios under various magnetic field configurations, including tokamaks, stellarators, and RFP devices.[29] By utilizing HPI2, we studied the pellet fueling depth with various injection parameters in a typical H-mode discharge on EAST. Corresponding results will be a reference to the upgrade of EAST's pellet injection system.

2.2. Initial setup

Inputs for HPI2 code include mainly the plasma temperature and density profiles, 2D magnetic geometry, q (safety factor) profile, and pellet injection parameters. The outputs that are of interest include mainly pellet ablation and deposition profiles. In addition, details of plasmoid evolution, including the dimensions of an ablation cloud, plasmoid density and ion and electron temperatures, can also be obtained.

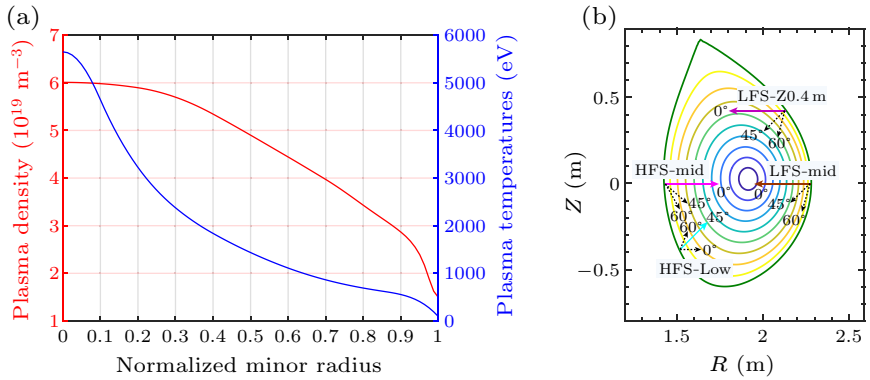


Fig. 1. (a) Fitted plasma density (red line), and temperature (blue line) profiles with experimental data from a typical H-mode discharge on the EAST tokamak. The edge electron density is measured with the reflectometer, and the fitting of the core density profile is constrained by the line-integrated density provided by POINT. The electron temperature is measured with Thomson scattering. (b) Plasma equilibrium reconstructed by EFIT, and the pellet paths (arrows) mapped onto magnetic flux surfaces for different injection geometries considered in this paper, including LFS-Z0.4m, LFS-mid, HFS-mid, and HFS-low. The green line represents the last closed flux surface (LCFS). The arrow lines mainly represent the adoption of three different injection angles for each of the four selected injection locations. A spherical pellet with radius of $r_p = 0.8, 1.0, 1.2$ mm and velocity of $V_p = 100$–300 m·s^{-1} is used in our simulations.

In the present study, a typical H-mode discharge in EAST is chosen as background plasma for the pellet injection of interest. Figure 1(a) shows the fitted electron temperature and density profiles of background plasma. The central electron density and temperature are $n_{e0} = 6.1 \times 10^{19}$ m^{-3} and $T_{e0} = 5.61$ keV, respectively. In addition, the pre-cooling effect is considered. The simulation domain is inside the last closed flux surface. The simulation grids are rectangular grids in (R, Z) coordinates, with the distance between two simulation grids chosen as $\mathrm{d}R = \mathrm{d}Z = 5$ mm. The pellet trajectory is mapped on 2D magnetic flux surface geometry, on which pellet ablation and plasmoid homogenization processes are simulated. The evolution of the ablation cloud parameters is described by a two-cell four-fluid model, which is essentially a 0D model, yet it still takes into account the actual tokamak configuration in a subtle way. For example, magnetic shear is considered when evolving the shape of the poloidal cross-section of the plasmoid.

A high-frequency and relatively low-frequency pellet injection system has been developed for the EAST device.[16,37] The preparation of deuterium pellets of high-frequency pellet injection system involves freezing hydrogen gas and cutting the ice into cylindrical shapes with a length of approximately 1.2 mm and a diameter of about 1.5 mm.[14] With approximation of a spherical shape for the pellet in the simulation, a simple estimate yields an equivalent radius of 0.8 mm with reference to the pellet injection parameters used in EAST experiments. We perform scans for pellet injection parameters to examine the parameter dependence of the pellet fueling depth.

Figure 1(b) shows the poloidal locations and angles of pellet injection considered in our simulation. In the real experiments, the injected location of pellet is 0.4 m above the middle plane of the low field side (LFS-Z0.4m) and 0.468 m below the middle plane of the high field side (HFS-low), respectively, with a horizontal velocity of about 110 m·s^{-1}. Besides the LFS-Z0.4m and HFS-low injection locations in the real experiment, we also considered other locations, including the middle plane of LFS (LFS-mid) and HFS (HFS-mid). At each location, three injection angles are mainly scanned in our simulation. The corresponding pellet injection geometry parameters are summarized in Table 1. In addition, in our simulation, pellets are assumed to be spherical with the pellet radius of $r_p = 0.8$, 1.0, 1.2 mm, respectively, corresponding to nominal pellet particle number $N_p = 1.29, 2.52, 4.36 \times 10^{20}$ atoms, respectively, and the pellet injection speed V_p is in the range of 100–300 m·s^{-1}.

Table 1. The injection parameters used in our simulations.

Locations	R (m)	Z (m)	$\alpha_{\mathrm{injection}}$
LFS-Z0.4m	2.35	0.40	0°, 45°, 60°
LFS-mid	2.35	0	0°, 45°, 60°
HFS-mid	1.51	0	0°, 25°, 40°, 45°,50°, 60°
HFS-low	1.35	−0.468	0°, 25°, 40°, 45°, 50°, 60°

3. Results and discussion

3.1. Pellet ablation and deposition

Pellet ablation and deposition are two main processes influencing pellet fueling efficiency. Pellet ablation is a fast process that takes place in mere microseconds, forming a plasmoid, and then particle deposition takes place in the process

of plasmoid movement, which results mainly from the ∇B-induced drift as mentioned in Section 1. Overall, this entire process typically takes around one millisecond. In Fig. 2, pellet ablation (solid lines) and deposition (dashed lines) profiles predicted with HPI2 code are shown for LFS-Z0.4m case, with various pellet injection angles, pellet injection speeds and sizes. In this study, the radial positions of the ablation profile peak and deposition profile peak are taken to characterize the pellet penetration depth and deposition depth (or fueling depth) respectively. For example, with parameters of a pellet injection velocity of 300 m/s and a radius of 0.8 mm, the penetration depths are $\rho = 0.65$, 0.68, 0.73 and the deposition depths are $\rho = 0.925$, 0.926, 0.938, respectively, at three different injection angles. By comparing the results with all combinations of pellet speeds and sizes at three different injection angles, i.e., 0° (red lines), 45° (blue lines), and 60° (green lines), it is clearly seen that the pellet fueling depth is the deepest with the injection angle of 45°. Deep fueling usually results in high fueling efficiency. Therefore, the simulation results indicate that 45° represents the most suitable pellet injection angle at the injection location of LFS-Z0.4m in three injection angles.

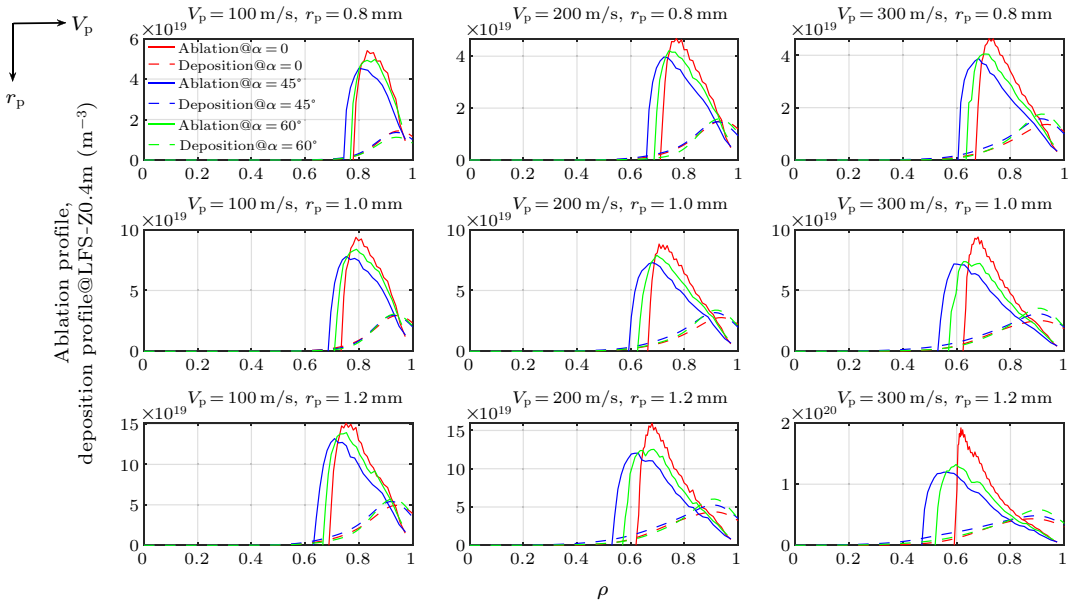


Fig. 2. Pellet ablation (solid lines) and deposition (dashed lines) profiles predicted with HPI2 code in LFS-Z0.4m injection case, with various pellet injection angles, pellet injection speeds and radius. The horizontal axis, ρ, is the normalized minor radius. The red, blue, and green lines correspond to injection angles of 0°, 45°, and 60°, respectively. The pellet injection speeds used in the simulation are 100 m·s^{-1}, 200 m·s^{-1}, and 300 m·s^{-1}, with pellet radius of 0.8 mm, 1.0 mm, and 1.2 mm, respectively.

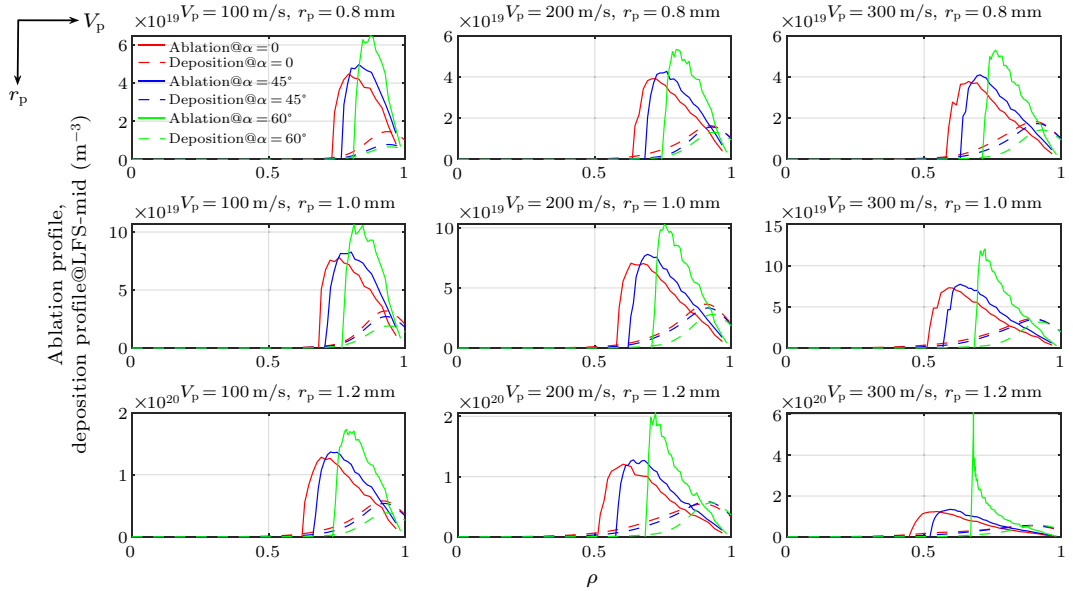


Fig. 3. Pellet ablation (solid lines) and deposition (dashed lines) profiles predicted with HPI2 code in the LFS-mid injection case, with various pellet injection angles, pellet injection speeds and radius. The horizontal axis, ρ, is the normalized minor radius. The red, blue, and green lines correspond to injection angles of 0°, 45°, and 60°, respectively. The pellet injection speeds used in the simulation are 100 m·s^{-1}, 200 m·s^{-1}, and 300 m·s^{-1}, with pellet radius of 0.8 mm, 1.0 mm, and 1.2 mm, respectively.

In Fig. 3, pellet ablation (solid lines) and deposition (dashed lines) profiles predicted with HPI2 code are shown for the LFS-mid case, with the same range of pellet injection parameters as shown in Fig. 2. By comparing results with three different injection angles, i.e., 0° (red lines), 45° (blue lines), and 60° (green lines), it is clearly seen that the pellet fueling depth is the deepest with the injection angle of 0°. This suggests that 0° is an optimal injection angle at the injection location of LFS-mid regardless of instability issues.

In Fig. 4, pellet ablation (solid lines) and deposition (dashed lines) profiles predicted with HPI2 code are shown for the HFS-mid case, with the same range of pellet injection parameters as shown in Fig. 2. By comparing results with three different injection angles, i.e., 0° (red lines), 45° (blue lines), and 60° (green lines), it is clearly seen that the pellet fueling depth is the deepest with the injection angle of 0°. It should be noted that increasing the injection speed and size both leads to deeper pellet penetration, which however may cause tangential singularity problems in calculating the ablation profile when the trajectory of the pellet aligns with certain magnetic flux surface. An areal deposition model developed in Ref. [23] can solve this issue. As in the LFS-mid injection case, the simulation results indicate that horizontal injection is the most suitable for the pellet injection location of HFS-mid.

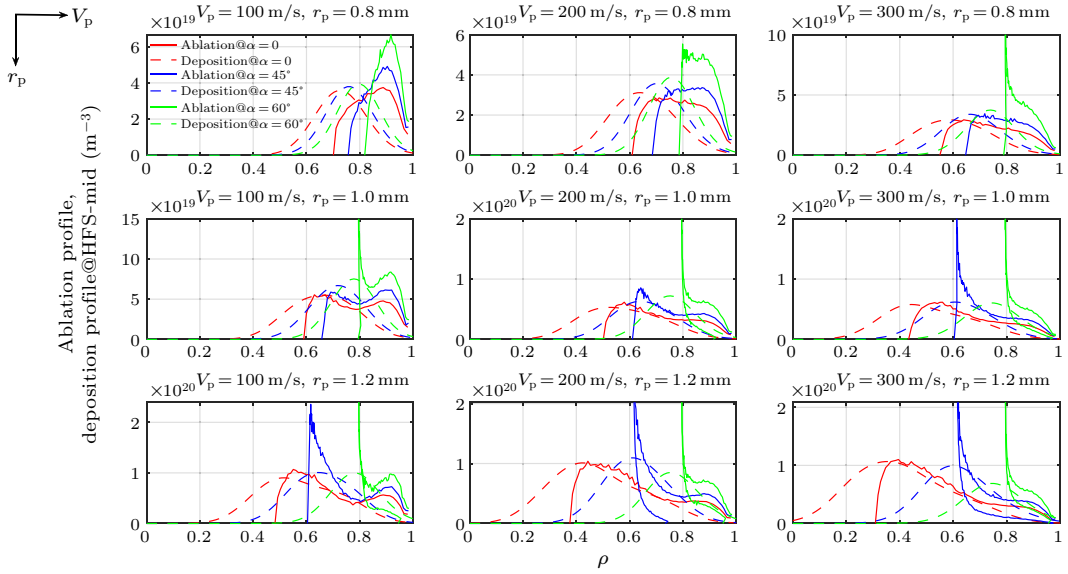


Fig. 4. Pellet ablation (solid lines) and deposition (dashed lines) profiles predicted with HPI2 code in the HFS-mid injection case, with various pellet injection angles, pellet injection speeds and radius. The horizontal axis, ρ, is the normalized minor radius. The red, blue, and green lines correspond to injection angles of 0°, 45°, and 60°, respectively. The pellet injection speeds used in the simulation are 100 m·s^{-1}, 200 m·s^{-1}, and 300 m·s^{-1}, with pellet radius of 0.8 mm, 1.0 mm, and 1.2 mm, respectively.

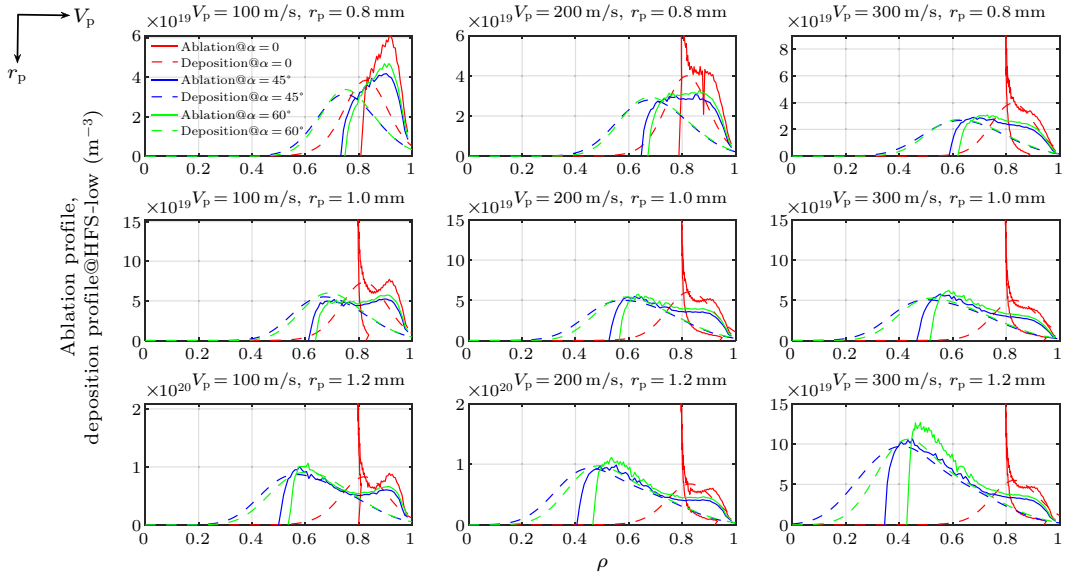


Fig. 5. Pellet ablation (solid lines) and deposition (dashed lines) profiles predicted with HPI2 code in the HFS-low injection case, with various pellet injection angles, pellet injection speeds and radius. The horizontal axis, ρ, is the normalized minor radius. The red, blue, and green lines correspond to injection angles of 0°, 45°, and 60°, respectively. The pellet injection speeds used in the simulation are 100 m·s^{-1}, 200 m·s^{-1}, and 300 m·s^{-1}, with pellet radii of 0.8 mm, 1.0 mm, and 1.2 mm, respectively.

Pellet ablation (solid lines) and deposition (dashed lines) profiles predicted with HPI2 code are shown for the HFS-low case in Fig. 5, with the same range of pellet injection parameters shown in Fig. 2. The tangential singularity problem is also encountered in calculating the ablation profile when the pellet trajectory is oblique and becomes tangent to certain magnetic flux surface. By comparing the results with three different injection angles, i.e., 0° (red lines), 45° (blue lines), and 60° (green lines), it is clearly seen that the pellet fueling depth is the deepest with the injection angle of 45°. Therefore, the simulation results suggest that an injection angle of 45° is an optimal choice at the injection location of HFS-low.

3.2. Electron density and temperature after pellet injection

Effects of pellet injection on plasma are studied by analyzing the predicted electron density and temperature profiles immediately after the pellet injection. Specifically, the pellet injection effectively leads to an increased density of the background plasma and also leads to a decrease in the background plasma temperature due to the cooling by the cold ablated particles. In Fig. 6 we compare two cases in which pellets are injected at the locations of LFS-Z0.4m [Figs. 6(a) and 6(b)] and HFS-low [Figs. 6(c) and 6(d)], respectively. These two locations are the currently adopted injection locations on the EAST device. Pellets can only be injected horizontally up to date. For future updates, the injection angle can be optimized based on our simulations. A 1.0 mm spherical deuterium pellet with a velocity of 300 m·s^{-1} is used in these two simulations.

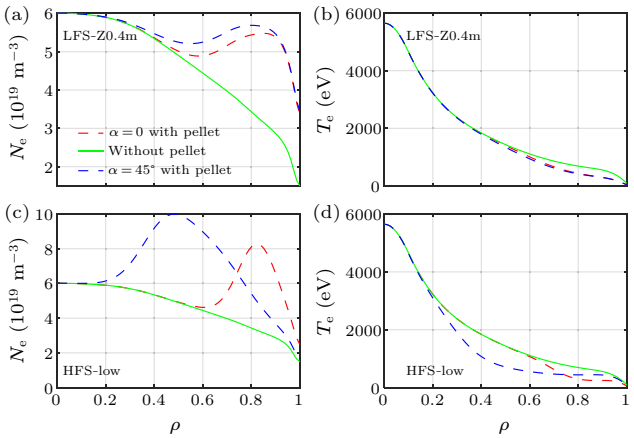


Fig. 6. Electron density and temperature profiles before (solid lines) and immediately after (dashed lines) pellet injection for [(a), (b)] the LFS-Z0.4m injection case and [(c), (d)] the HFS-low injection case, respectively. The dashed lines of red and blue correspond to injection angles of 0° and 45°, respectively.

The simulation results shown in Figs. 6(a) and 6(c) indicate that the electron density is influenced more significantly by pellet injection at the HFS-low location than at the LFS-Z0.4m injection location. The pellet fueling efficiency is higher at HFS due to the inward drift of plasmoids, while it is much lower at LFS due to the loss of particles induced by the outward drift of plasmoids. Thus, in the HFS-low injection case, the pellet injected at an injection angle of 45° leads to deeper fueling than that injected at an angle of 0°, which is consistent with the corresponding deposition profiles as shown in Fig. 8. This confirms that the choice of injection angle of about 45° is expected to achieve deep fueling depth and high fueling efficiency for the HFS-low injection case. Since the pellet is made up of a frozen material, injecting it into the background plasma leads to a decrease in electron temperature. In HPI2, it is assumed that the background plasma is adiabatically cooled by the deposited pellet particles. Comparison of electron temperature after pellet injection in Figs. 6(c) and 6(d) shows that the pellet causes less perturbation on the electron temperature injected at the LFS-Z0.4m location than that injected at the HFS-low location. Because the cooling effect is stronger in the latter case due to its high fueling efficiency.

3.3. Fueling depth dependence on pellet velocity and size

The velocity and size of pellet influence pellet fueling depth through their impact on both pellet ablation and plasmoid drift. While it is apparent that the penetration depth of pellet increases with increased pellet velocity and size, their impact on plasmoid drift is indirect. With a larger size and a higher velocity, a pellet penetrates deeper, reaching a region with higher plasma temperature. The plasmoid formed at this region is heated faster, increasing the plasmoid pressure and leads to an enhanced drift of the plasmoid. In other words, pellet injection with larger size and higher velocity usually leads to higher fueling efficiency, because of not only the increased penetration depth but also larger drift displacements of those plasmoids formed at core region. The enhanced plasmoid drifts can also be inferred from Figs. 2–5, by comparing the differences between deposition and ablation profiles with different pellet sizes and velocities.

However, it should be pointed out that one cannot conclude that larger pellet size with higher velocity must lead to higher fueling efficiency, because the pellet with large size may penetrate across the magnetic axis or penetrate through the whole plasma with too high velocity, especially in the cases with oblique injection, such as the 60° injection case at HFS-mid and 0° injection case at HFS-low as shown in Figs. 4 and Fig. 5, respectively. In these two cases, the pellet with too large radius or too high speed penetrates through the plasma without being fully ablated. The integration of the density increment in such cases are smaller than those cases where pellets are fully ablated. In addition, too large pellet may lead to some plasma instability, and too high speed may put a challenge to pellet injection technology, especially in the HFS injection cases, where curved tubes are needed to transfer pellets to the injection position. Therefore, it is necessary to control the ve-

locity and size of the pellets within a reasonable range. In conclusion, the optimization of pellet fueling depth and fueling efficiency requires considering further constraints by other physics aspects such as plasma instability and engineering aspect.

3.4. Fueling dependence on pellet injection angles

From Figs. 2–5, it is seen that the pellet has deeper fueling depth when injected on HFS compared to LFS. In this section, we further investigate the influence of injection angles on pellet fueling depth. Simulations were conducted with a fixed pellet injection velocity of 100 m/s and a radius of 1.0 mm, at HFS-mid and HFS-low positions, respectively. In addition to angles of 0°, 45°, and 60°, we consider three additional angles of 25°, 40°, and 50°.

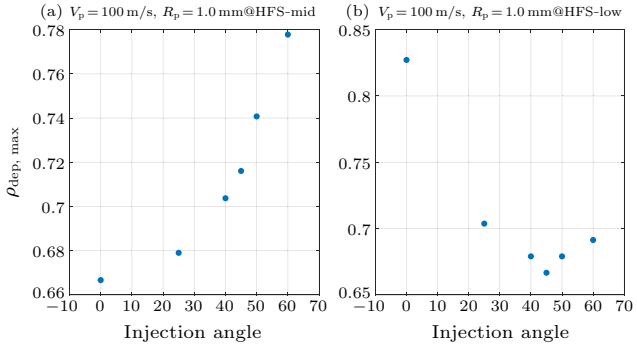


Fig. 7. Fueling depth predicted with HPI2 code with pellets injected at HFS-mid (a) and HFS-low (b) respectively, with various pellet injection angles. The pellet injection speed used in the simulation is 100 m·s^{-1}, with a pellet radius of 1.0 mm.

The predicted penetration depths are $\rho = 0.67$, 0.68, 0.70, 0.71, 0.74, and 0.77, respectively, with angles 0°, 25°, 40°, 45°, 50°, and 60°, when the pellet is injected at HFS-mid, as shown in Fig. 7(a). With decreasing injection angles, the particle deposition depth gradually moves towards the core position. Therefore, for HFS-mid injection, it is recommended to perform horizontal injection to have the deepest fueling depth. Similarly, from Fig. 7(b), we conclude that the pellet should be injected at an angle of 45° at HFS-low position to achieve deep fueling depth.

3.5. The pre-cooling effect on pellet fueling depth

As mentioned above, plasmoids drift along the direction of the major radius, and the drift speed is usually much higher than the pellet speed. Deposition of cold plasmoid particles drifting in front of the pellet will cause the pre-cooling of the background plasma in the HFS injection cases. The pellet that penetrates here later on will feel lower temperature, and thus the pellet ablation rate is decreased and penetration depth is deeper. The pre-cooling effect provides a reasonable explanation for the experimental observation that the pellet penetration depth is usually significantly larger on the HFS compared to the LFS.[38] Deposition of ablated particles in a plasmoid drifting in front of the pellet is modelled with the drift and homogenization model described in Subsection 2.1. The cooling of the background plasma is modelled as an adiabatic process in HPI2.

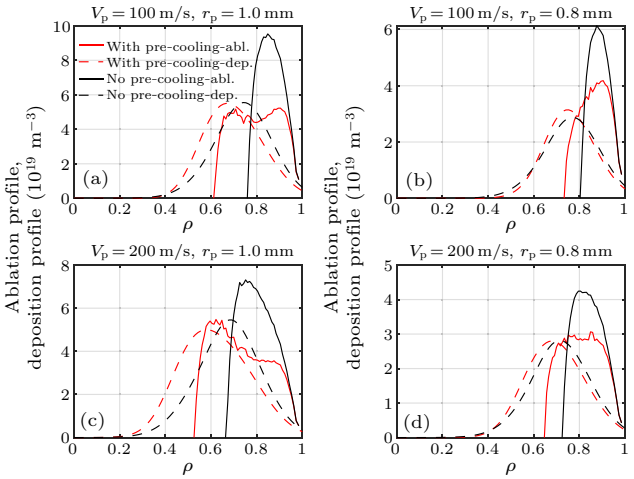


Fig. 8. The predicted profiles of pellet ablation (solid lines) and deposition (dashed lines) obtained with HPI2 with pre-cooling effect (red lines) and without pre-cooling effect (black lines). The injection location of the pellet is HFS-low with an injection angle of 45°. [(a), (b)] For the cases with the pellet injection speed of 100 m/s and radius of 1.0 mm and 0.8 mm, respectively. [(c), (d)] For the cases with the pellet injection speed of 200 m/s and radius of 1.0 mm and 0.8 mm, respectively.

Figure 8 shows the predicted profiles of pellet ablation (solid lines) and deposition (dashed lines) obtained with HPI2 with (red lines) and without pre-cooling effect (black lines), respectively. HFS-low is chosen as the injection location, with an injection angle of 45°, since it may represent the most suitable injection angle at this location as mentioned in Subsection 3.2. The radius of pellet used in simulation is 0.8 mm and 1.0 mm and the injection speed is 100 m/s and 200 m/s.

The simulation results suggest that taking into account pre-cooling effect may have a significant impact on pellet ablation rate and penetration depth. When the pre-cooling effect is considered, the pellet ablation rate is greatly reduced, leading to a broaden ablation profile, as shown by the solid red lines. Correspondingly, the peak of the ablation profile is lower compared to the case in which the pre-cooling effect is not considered. However, the deposition depth of the pellet increases only slightly when taking into account the influence of the pre-cooling effect, especially for small pellets as shown in Figs. 8(b) and 8(d). The simulation results show the similar trends for pellets with different velocities, ranging from 100 m/s [Figs. 8(a) and 8(b)] to 200 m/s [Figs. 8(c) and 8(d)].

The pre-cooling effect has a more noticeable impact on penetration depth than on deposition depth because plasmoid drifts are smaller when pre-cooling effect is taken into account. This can be clearly seen in Fig. 9, in which drift distances of plasmoids at the same radial position are compared with (red lines) and without (black lines) taking into account pre-cooling effect. When including pre-cooling effect, the ablation rate be-

comes lower, resulting in a lower plasmoid density. In addition, the temperature of the background plasma, cooled by the deposition of previously formed plasmoids, becomes lower. These two effects lead to a lower plasmoid pressure, which is the driving term of the ∇B-induced drift. Therefore, plasmoid drift distances decrease compared to the case without taking into account the pre-cooling effect. Further research is needed to investigate in detail how the pre-cooling effect affects the evolution of plasmoid parameters, which is left as the future work.

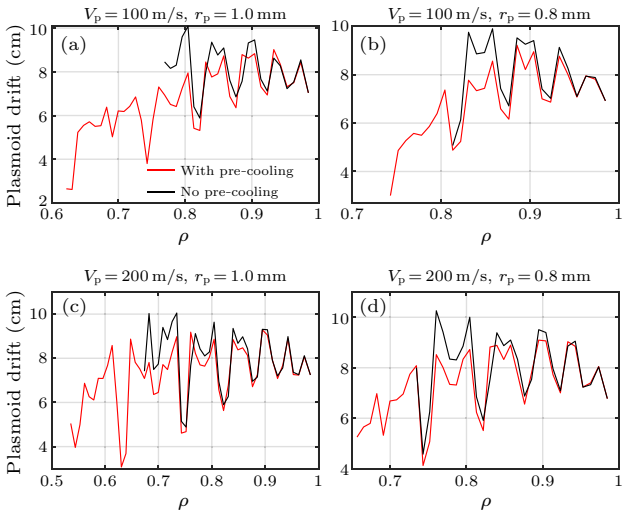


Fig. 9. The plasmoid drift displacements predicted by the HPI2 code versus the normalized minor radius with (red lines) and without (black lines) pre-cooling effect. [(a), (b)] For the cases with the pellet injection speed of 100 m/s and radius of 1.0 mm and 0.8 mm, respectively. [(c), (d)] For the cases with the pellet injection speed of 200 m/s and radius of 1.0 mm and 0.8 mm, respectively.

3.6. Discussion

Simulation results indicate a systematically deeper pellet deposition depth, which usually gives a higher fueling efficiency, when the pellet injection location is selected on the HFS compared to the LFS. The result is consistent with the experimental observations on ASDEX-Upgrade, Tore Supra, DIII-D, and EAST. For quantitative comparison, in an ASDEX-Upgrade experiment, the averaged plasmoid drift displacement was determined on the order of 10 cm, while the drift displacement obtained on the EAST tokamak with similar plasma and pellet injection parameters is approximately 8 cm, as shown in Fig. 9.[8,16,35,39–41] However, in previous studies, the impact of pellet injection angles on the pellet deposition depth has not been explored, partly because of the difficulty in changing the injection angle at an injection position due to engineering constraints. Therefore, we conducted scan of pellet injection parameters including the injection angle. From simulation point of view, four pellet injection positions are selected with three different injection angles at each position. Simulation results indicate that injecting pellets at HFS middle plane with 0° injection angle leads to the highest deposition depth. However, it is important to note that performing pellet injection at HFS middle plane location with a small injection angle such as 0°, is technically very challenging from an engineering perspective. On the other hand, it is noted that pellet injection at HFS-low with 45° injection angle gives comparable deposition depths with pellets injected at HFS middle plane with 0° injection angle. Therefore, for the design of the next-generation pellet injection system for EAST, using a curved tube to deliver pellets to the HFS-low position and injecting them at an angle of 45°, can potentially achieve deep pellet deposition. It should be pointed out that this study only considers thermal electrons and ions when predicting pellet ablation and deposition profiles, without taking into account the ablation enhancement caused by fast electrons or fast ions generated by auxiliary heating and current-driven methods, such as LHCD and NBI. These will be considered in the future work.

4. Conclusions

In summary, the advanced hydrogen isotopes pellet injection code HPI2 has been utilized to evaluate the pellet fueling depth on the EAST device. We study pellet ablation and deposition at various poloidal injection locations and angles by scans of these parameters. The simulation results indicate that the pellet injection penetration is notably deeper when pellets are injected at an HFS location, compared with at an LFS location. At a selected injection location, we mainly study the cases at three different injection angles of 0°, 45°, and 60°. When injection locations are on the middle plane of LFS or HFS, it is found that a good pellet injection angle is along the middle plane. However, if the injection location is 0.4 m above the middle plane in the LFS case or 0.468 m below the middle plane in the HFS case, an ideal pellet injection angle is close to 45°. In general, the deeper penetration depth can be obtained with injection angles perpendicular or nearly perpendicular to the magnetic flux surfaces. This study can help in optimizing and finding the best combination of pellet injection parameters such as injection locations and angles.

Acknowledgments

This work was supported by the National Natural Science Foundation of China (Grant Nos. 12205196 and 12275040) and the National Key Research and Development Program of China (Grant No. 2022YFE03090003).

References

[1] Kukushkin A S, Polevoi A R, Pacher H D, Pacher G W and Pitts R A 2011 *J. Nucl. Mater.* **415** S497

[2] Wu X, Li H, Wang Z, Feng H and Zhou Y 2017 *Chin. Phys. B* **26** 065201

[3] Parail V, Belo P, Boerner P, Bonnin X, Corrigan G, Coster D, Ferreira J, Foster A, Garzotti L, Hogeweij G M D, Houlberg W, Imbeaux F, Johner J, Kochl F, Kotov V, Lauro-Taroni L, Litaudon X, Lonnroth J, Pereverzev G, Peysson Y, Saibene G, Sartori R, Schneider M, Sips G, Strand P, Tardini G, Valovic M, Wiesen S, Wischmeier M and Zagorski R 2009 *Nucl. Fusion* **49** 075030

[4] McCarthy K J, Panadero N, Combs S K, Tamura N, Ascasibar E, Calvo M, Chmyga A, Estrada T, Fontdecaba J M, Garcia R, Hernández Sánchez J, Khabanov P, Liners M, Melnikov A V, Pastor I and Rojo B 2019 *Plasma Phys. Control. Fusion* **61** 014013

[5] Milora S L, Houlberg W A, Lengyel L L and Mertens V 1995 *Nucl. Fusion* **35** 657

[6] Parks P B and Baylor L R 2005 *Phys. Rev. Lett.* **94** 125002

[7] Li M, Sun J, Wang Y and Xia T 2021 *Nucl. Mater. Energy* **26** 100888

[8] Baylor L R, Jernigan T C, Parks P B, Antar G, Brooks N H, Combs S K, Fehling D T, Foust C R, Houlberg W A and Schmidt G L 2007 *Nucl. Fusion* **47** 1598

[9] Futatani S, Huijsmans G, Loarte A, Baylor L R, Commaux N, Jernigan T C, Fenstermacher M E, Lasnier C, Osborne T H and Pegourié B 2014 *Nucl. Fusion* **54** 073008

[10] Lang P T, Nakano T, Davis S, Matsunaga G, Pégourié B, Ploeckl B and Treuterer W 2019 *Fusion Eng. Des.* **146** 91

[11] Xu H B, Zhu G L, Liu D Q, Vinyar I, Wang M J and Lukin A 2012 *Fusion Sci. Technol.* **62** 316

[12] Pégourié B and Géraud A 2009 *Fusion Sci. Technol.* **56** 1318

[13] Reksoatmodjo R, Mordijck S, Hughes J W, Lore J D and Bonnin X 2021 *Nucl. Mater. Energy* **27** 100971

[14] Hou J, Hu J, Chen Y, Wang Y, Zang Q, Xu J, Liu H, Tritz K, Gilson E, Yuan X, Sun Z, Maingi R, Zhao H and Li J 2019 *Fusion Eng. Des.* **145** 79

[15] Chen W T, Sun J Z, Gao F, Peng L and Wang D Z 2022 *Chin. Phys. B* **31** 075204

[16] Li C Z, Hu J S, Chen Y, Vinyar I V, Li J G and Lukin Y 2014 *Fusion Eng. Des.* **89** 99

[17] Hou J, Chen Y, Zuo G, Hu J, Mao S, Yuan X, Huang J, Wu M, Xu L, Zhao H, Yuan J, Wang S, Liu H, Meng L, Shi T, Li P and Li J 2022 *Plasma Phys. Control. Fusion* **64** 055010

[18] Parks P B and Turnbull R J 1978 *Phys. Fluids* **21** 1735

[19] Pégourié B, Waller V, Dumont R J, Eriksson L G, Garzotti L, Géraud A and Imbeaux F 2005 *Plasma Phys. Control. Fusion* **47** 17

[20] Gao F, Sun J, Sun Z, Zuo G, Hu J, Loarte A, Bonnin X, Peng L and Liu J 2020 *Nucl. Fusion* **60** 066022

[21] Sun J, Liu L, Sun Z, Li M, Li N and Wang D 2018 *Fusion Eng. Des.* **136** 834

[22] McClenaghan J, Lao L, Parks P, Wu W, Zhang J and Chan V 2023 *Nucl. Fusion* **63** 036015

[23] Zhang J and Parks P 2020 *Nucl. Fusion* **60** 066027

[24] Zhang J, McClenaghan J, Parks P, Lao L and Wu W 2022 *Nucl. Fusion* **62** 086012

[25] Houlberg W A and Attenberger S E 1988 *Nucl. Fusion* **28** 595

[26] Garzotti L, Pégourié B, Géraud A, Frigione D and Baylor L R 1997 *Nucl. Fusion* **37** 1167

[27] Artaud J F, Basiuk V, Imbeaux F, Schneider M, Garcia J, Giruzzi G, Huynh P, Aniel T, Albajar F, Ané J M, Bécoulet A, Bourdelle C, Casati A, Colas L, Decker J, Dumont R, Eriksson L G, Garbet X, Guirlet R, Hertout P, Hoang G T, Houlberg W, Huysmans G, Joffrin E, Kim S H, Köchl F, Lister J, Litaudon X, Maget P, Masset R, Pégourié B, Peysson Y, Thomas P, Tsitrone E and Turco F 2010 *Nucl. Fusion* **50** 043001

[28] Kalupin D, Ivanova-Stanik I, Voitsekhovitch I, Ferreira J, Coster D, Alves L L, Aniel T, Artaud J F, Basiuk V, Bizarro J P S, Coelho R, Czarnecka A, Huynh P, Figueiredo A, Garcia J, Garzotti L, Imbeaux F, Köchl F, Nave M F, Pereverzev G, Sauter O, Scott B D, Stankiewicz R and Strand P 2013 *Nucl. Fusion* **53** 123007

[29] Geulin E and Pégourié B 2022 *Plasma Fusion Res.* **17** 2102101

[30] Pégourié B and Dubois M A 1989 *Nucl. Fusion* **29** 745

[31] Pégourié B and Picchiottino J M 1996 *Phys. Plasmas* **3** 4594

[32] Pégourié B, Waller V, Nehme H, Garzotti L and Géraud A 2007 *Nucl. Fusion* **47** 44

[33] Köchl F, Pegourie B, Matsuyama A, Nehme H, Waller V, Frigione D, Garzotti L, Kamelander G, Parail V and JET EFDA 2012 *Modelling of Pellet Particle Ablation and Deposition: The Hydrogen Pellet Injection code HPI2* EUROfusion Prepr EFDA-JET-PR(12)57

[34] Parks P B, Sessions W D and Baylor L R 2000 *Phys. Plasmas* **7** 1968

[35] Pégourié B 2007 *Plasma Phys. Control. Fusion* **49** R87

[36] Rozhansky V, Senichenkov I, Veselova I and Schneider R 2004 *Plasma Phys. Control. Fusion* **46** 575

[37] Hu J S, Sun Z, Li C Z, Zhen X W, Li J G, Guo H Y, Li J H, Wang L, Gan K F, Chen Y, Ren J, Zuo G Z, Yao X J, Hu L Q, Gong X Z, Wan B N, Zou X L, Mansfield D K, Liang Y F and Vinyar I 2015 *J. Nucl. Mater.* **463** 718

[38] Lang P T, Büchl K, Kaufmann M, Lang R S, Mertens V, Müller H W and Neuhauser J 1997 *Phys. Rev. Lett.* **79** 1487

[39] Hou J, Chen Y, Yuan X, Limeng M, Sun Z, Zuo G and Hu J 2020 *Fusion Eng. Des.* **153** 111482

[40] Hou J, Chen Y, Vinyar I, Yuan X and Hu J 2018 *Fusion Eng. Des.* **130** 69

[41] Müller H W, Dux R, Kaufmann M, Lang P T, Lorenz A, Maraschek M, Mertens V and Neuhauser J 2002 *Nucl. Fusion* **42** 301